Journal of Advanced Research xxx (xxxx) xxx

Contents lists available at ScienceDirect

Journal of Advanced Research

journal homepage: www.elsevier.com/locate/jare

Multifunctional derivatives of pyrimidine-5-carbonitrile and differently substituted carbazoles for doping-free sky-blue OLEDs and luminescent sensors of oxygen

Uliana Tsiko [a], Oleksandr Bezvikonnyi [a], Galyna Sych [a], Rasa Keruckiene [a], Dmytro Volyniuk [a], Jurate Simokaitiene [a], Iryna Danyliv [b], Yan Danyliv [b], Audrius Bucinskas [a], Xiaofeng Tan [a], Jouzas Vidas Grazulevicius [a,*]

[a] Department of Polymer Chemistry and Technology, Kaunas University of Technology, Radvilenu pl. 19, LT-50254 Kaunas, Lithuania
[b] Department of Electronic Devices, Lviv Polytechnic National University, S. Bandera 12, 79013 Lviv, Ukraine

HIGHLIGHTS

- Pyrimidine-5-carbonitrile-based compounds with efficient TADF exceeding reverse intersystem crossing rates of 10^6 s^{-1}.
- AIEE properties for the designed compounds allowing to reach PLQYs up to 50% in solid state.
- Bipolar charge-transporting properties showing hole mobility of 1.6×10^{-4} $cm^2/V{\cdot}s$ and electron mobility of 1.37×10^{-5} $cm^2/V{\cdot}s$.
- Non-doped sky-blue OLED with external quantum efficiency of 12.8%.
- Oxygen probes with fast response, high sensitivity and good stability.

GRAPHICAL ABSTRACT

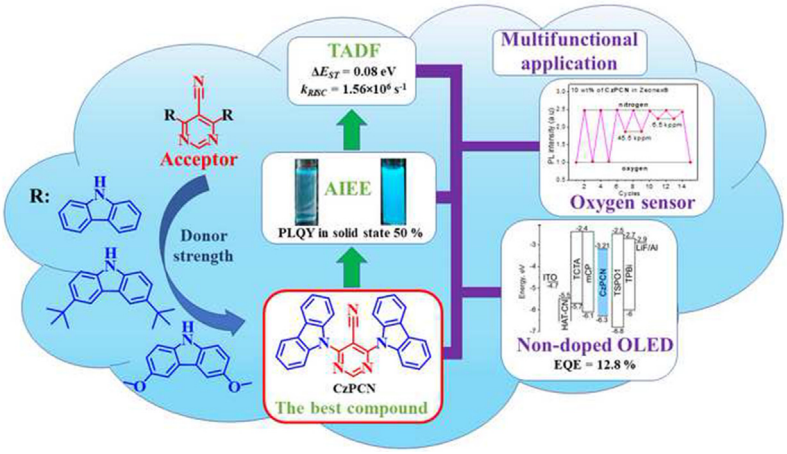

ARTICLE INFO

Article history:
Received 15 October 2020
Revised 6 January 2021
Accepted 23 January 2021
Available online xxxx

Keywords:
Organic light-emitting diode
Optical sensor
Pyrimidine-5-carbonitrile
Carbazole, Thermally activated delayed fluorescence
Aggregation-induced emission enhancement

ABSTRACT

Introduction: Evolution of organic light-emitting diodes (OLEDs) reached the point, which allows to obtain maximum internal quantum efficiency of 100% partly using heavy-metal-free emitters exhibiting thermally activated delayed fluorescence (TADF). Such emitters are also predictively perfect candidates for new generation of optical sensors since triplet harvesting can be sensitive to different analytes (at least to oxygen). Although many organic TADF emitters have been reported so far as OLED emitters, the investigation of materials suitable for both OLEDs and optical sensors remains extremely rare.

Objectives: Aiming to achieve high photoluminescence quantum yields in solid-state and triplet harvesting abilities of organic semiconductors with efficient bipolar charge transport required for application in both blue OLEDs and optical sensors, symmetrical donor–acceptor-donor organic emitters containing pyrimidine-5-carbonitrile electron-withdrawing scaffold and carbazole, *tert*-butylcarbazole and methoxy carbazole donor moieties were designed, synthesized and investigated as the main objectives of this study.

Methods: New compounds were tested by many experimental methods including optical and photoelectron spectroscopy, time of flight technique, electrochemistry and thermal analyses.

Peer review under responsibility of Cairo University.

* Corresponding author.
E-mail address: juozas.grazulevicius@ktu.lt (J.V. Grazulevicius).

https://doi.org/10.1016/j.jare.2021.01.014
2090-1232/© 2021 Production and hosting by Elsevier B.V. on behalf of Cairo University.
This is an open access article under the CC BY-NC-ND license (http://creativecommons.org/licenses/by-nc-nd/4.0/).

Please cite this article as: U. Tsiko, O. Bezvikonnyi, G. Sych et al., Multifunctional derivatives of pyrimidine-5-carbonitrile and differently substituted carbazoles for doping-free sky-blue OLEDs and luminescent sensors of oxygen, Journal of Advanced Research, https://doi.org/10.1016/j.jare.2021.01.014

Results: Demonstrating advantages of the molecular design, the synthesized emitters exhibited sky-blue efficient TADF with reverse intersystem crossing rates exceeding 10^6 s^{-1}, aggregation-induced emission enhancement with photoluminescence quantum yields in solid state exceeding 50%, hole and electron transporting properties with charge mobilities exceeding 10^{-4} $cm^2/V{\cdot}s$, glass-forming properties with glass transition temperatures reaching 177 °C. Sky-blue OLEDs with non-doped light-emitting layers of the synthesized emitter showed maximum external efficiency of 12.8% while the doped device with the same emitter exhibited maximum external efficiency of 14%. The synthesized emitters were also used as oxygen probes for optical sensors with oxygen sensitivity estimated by the Stern-Volmer constant of $3.24{\cdot}10^{-5}$ ppm^{-1}.

Conclusion: The developed bipolar TADF emitters with pyrimidine-5-carbonitrile and carbazole moieties showed effective applicability in both blue OLEDs and optical sensors.

© 2021 Production and hosting by Elsevier B.V. on behalf of Cairo University. This is an open access article under the CC BY-NC-ND license (http://creativecommons.org/licenses/by-nc-nd/4.0/).

Introduction

The technology of organic light emitting diodes (OLED) became one of the most expanding in the markets of displays and lighting devices [1,2]. The pressure-sensitive paint technique for luminescent sensors of oxygen is a widespread tool in various areas such as microelectronics and aerospace engineering [3–6]. Both luminescent sensor and OLED technologies require efficient metal-free emitters as an alternative of transition metals containing phosphorescent emitters which suffer from price-growing and ecological problems [7,8]. The attractive approach to solve this problems is usage of metal-free emitters exhibiting thermally activated delayed fluorescence (TADF) [9,10]. Employment of triplet excitons into luminescence of TADF emitters can break the limit of internal quantum efficiency of fluorescent OLEDs of 25% [11]. On the other hand, it is possible to use TADF emitters for fabrication of the sensors for oxygen due to the high sensitivity of excited triplet state of TADF molecules to the presence of oxygen in atmosphere [12–14]. For example, fullerene C_{70} was studied for the employment of TADF in oxygen sensing [15,16]. Potentially, TADF emitters can replace phosphorescent emissive species of electroluminescent oxygen pressure sensors. Electroluminescent pressure sensor based on oxygen quenching of electroluminescence was reported as an alternative to the conventional photoluminescent pressure-sensitive paint [17]. Taking into account that the biggest challenge of OLED technology is increase of efficiency of blue-emitting devices [18], the aim of this study was development of efficient multifunctional blue TADF emitters for OLEDs and optical sensors of oxygen.

To design efficient blue TADF emitters with appropriate charge-transporting properties required for OLEDs and with high photoluminescent quantum yields in solid-state required for both OLEDs and optical sensors, the following information was taken into account.

TADF occurs due to up-conversion of triplet excitons to the first singlet excited states through the mechanism of reverse intersystem crossing (RISC) [11]. It is facilitated by a thermal motion of atoms [19]. The small difference of energy levels between the first excited singlet (E_{S1}) and triplet (E_{T1}) excited states (ΔE_{ST}) is required for efficient RISC [20]. This condition is realized when overlap of the wavefunctions of HOMO and LUMO is minimized [21–23]. The optimal strategy for design of TADF emitters is a development of donor–acceptor or donor–acceptor-donor compounds in which HOMO is localized on an electron donating unit and LUMO is situated on an acceptor for the formation of charge transfer (CT) states [24–26].

From the investigations of Stokes reported in 1853 [27] till the introduction of the concept of aggregation-induced emission in 2001, compounds which exhibited more efficient emission in solid state than in solutions were known but they were not extensively studied [28,29]. The phenomenon of aggregation-induced emission enhancement (AIEE) is characterized by a significantly higher photoluminescence (PL) quantum yields (Φ) of the solid samples in which intramolecular vibrational and rotational motions are suppressed than of dilute solutions of compounds. Utilization of AIEE in OLEDs can help to overcome quenching of electroluminescence (EL) caused by π-π stacking in an emissive layer (EML). The promising recent area of research is development of TADF emitters exhibiting AIEE [30,31]. They are considered as promising candidates for non-doped EML of efficient OLEDs [32].

Emissive and charge-transporting properties of TADF compounds can be purposively modified by careful selection of donating and accepting moieties and the linking topology of them. Carbazole is one of the most widely used donor moieties in the design of TADF emitters [33]. Derivatives of carbazole exhibit high triplet energy, good thermal stability and hole transporting properties [11,34]. Attachment of *tert*-butyl or methoxy groups to carbazole moieties present in the molecules of emitters can lead to the suppression of the non-radiative paths of deactivation of excited states and an enhancement of TADF [26]. The increase of efficiency of TADF of the molecular mixture of cabazolyl disubstituted pyrimidine and bis[2-(diphenylphosphino)phenyl] ether oxide (DPEPO) was reached by attachment of *tert*-butyl and methyl groups to carbazole moieties [35]. The maximum value of external quantum efficiency (EQE) of the deep-blue OLED based on this molecular mixture was 8.4%. Pyrimidine-5-carbonitrile was utilized as an acceptor in TADF emitters providing uniform electron density distribution on the accepting moiety [36]. Green OLEDs based on pyrimidine-5-carbonitrile derivatives doped into 9-(30-(4,6-diphenyl-1,3,5-triazin-2-yl)-[1,10-biphenyl]-3-yl)-9H-carbazole host matrix showed EQE up to 19.8% [36]. However, blue TADF OLEDs with the emitters containing pyrimidine-5-carbonitrile acceptor moiety were not yet reported.

After analysis of the previously published approaches for efficient TADF emitters, we report on single-step synthesis and properties of new pyrimidine-5-carbonitrile and carbazole derivatives with donor–acceptor-donor structures aiming to develop efficient multifunctional blue emitters for OLEDs and optical sensors of oxygen. The obtained compounds demonstrated blue TADF and AIEE as well as high thermal and electrochemical stability and good charge-transporting properties that allowed to use them for fabrication of efficient doped and non-doped sky-blue OLEDs. In addition, the synthesized compounds were successfully utilized in highly sensitive and stable oxygen sensors. This is the first demonstration of oxygen sensing ability of pyrimidine-5-carbonitrile derivatives exhibiting TADF/AIEE.

Material and methods

General procedure of nucleophilic substitution reactions

Potassium hydroxide (2.5 eq.) was added to a solution of 9*H*-carbazole (2.5 eq.) or 3,6-di-*tert*-butyl-9H-carbazole (2.5 eq.) or

3,6-dimethoxy-9*H*-carbazole (2.5 eq.) in DMSO (25 ml). The mixture was stirred for 20 min at room temperature and then 4,6-dichloropyrimidine-5-carbonitrile (1 eq.) was added. The reaction mixture was heated to 175 °C and stirred for 1 h. After completion of the reaction, the obtained mixture was cooled down to room temperature, poured into water and filtered. The crude product was purified by column chromatography on silica gel using the eluent mixture of hexane and DCM with the volume ratio of 3:2 and recrystallized from isopropanol/DMF mixture.

4,6-Di(9*H*-carbazol-9-yl)pyrimidine-5-carbonitrile (CzPCN) was prepared from KOH (2.5 mmol, 0.28 g), 9*H*-carbazole (5 mmol, 0.84 g) and 4,6-dichloropyrimidine-5-carbonitrile (2 mmol, 0.35 g) using general procedure and yellow needle crystals were isolated in 49% yield (0.41 g). M.P.: 260–262 °C.

^{1}H NMR (400 MHz, $CDCl_3$) δ 9.34 (s, 1H), 8.06 (d, J = 7.7 Hz, 4H), 7.86 (d, J = 8.3 Hz, 4H), 7.58 – 7.48 (m, 4H), 7.39 (t, J = 7.4 Hz, 4H) ppm. ^{13}C NMR (101 MHz, $CDCl_3$) δ 161.86, 161.11, 138.46, 126.74, 125.91, 123.52, 120.71, 112.53, 112.36, 96.79 ppm. Elemental analysis: calculated for $C_{29}H_{17}N_5$, %: C, 79.98; H, 3.93; N, 16.08. Found, %: C 80.75; H 3.78; N 15.47. ESI-MS *(m/z)*: calculated for $C_{29}H_{17}N_5$, 435.48 $[M]^+$; found 457.99 $[M + Na]^+$.

4,6-bis(3,6-di-*tert*-butyl-9*H*-carbazol-9-yl)pyrimidine-5-carbonitrile (*t*CzPCN) was obtained according to general procedure from KOH (2.5 mmol, 0.28 g), 3,6-di-*tert*-butyl-9H-carbazole (5 mmol, 1.40 g) and 4,6-dichloropyrimidine-5-carbonitrile (2 mmol, 0.35 g) and yellow crystals was isolated in 36% yield (0.5 g). M.P.: 258–260 °C.

^{1}H NMR (400 MHz, $CDCl_3$) δ 9.23 (s, 1H), 8.04 (d, J = 1.5 Hz, 4H), 7.80 (d, J = 8.7 Hz, 4H), 7.57 (dd, J = 8.7, 1.8 Hz, 4H), 1.42 (s, 36H) ppm. ^{13}C NMR (101 MHz, $CDCl_3$) δ 161.81, 160.88, 146.63, 136.84, 126.10, 124.31, 116.75, 112.74, 112.33, 95.15, 34.96, 31.86 ppm. Elemental analysis: calculated for $C_{45}H_{49}N_5$, %: C, 81.90; H, 7.48; N, 10.6. Found, %: C 82.61; H 7.20; N 10.19. ESI-MS *(m/z)*: calculated for $C_{45}H_{49}N_5$, 659.90 $[M]^+$; found 682.51 $[M + Na]^+$.

4,6-bis(3,6-dimethoxy-9*H*-carbazol-9-yl)pyrimidine-5-carbonitrile (MeOCzPCN) was synthesized from KOH (2.5 mmol, 0.28 g), 3,6-dimethoxy-9*H*-carbazole (5 mmol, 1.14 g) and 4,6-dichloropyrimidine-5-carbonitrile (2 mmol, 0.35 g) by using general procedure and yellow crystals was isolated in yield 63% (0.7 g). M.P.: 286–288 °C.

^{1}H NMR (400 MHz, $(CD_3)_2SO$) δ 9.46 (s, 1H), 7.94 (d, J = 9.0 Hz, 4H), 7.88 (d, J = 2.3 Hz, 4H), 7.22 (dd, J = 9.0, 2.4 Hz, 4H), 3.94 (s, 12H) ppm. ^{13}C NMR (101 MHz, $(CD_3)_2SO$) δ 161.50, 156.21, 134.18, 133.48, 126.30, 115.56, 114.77, 104.15, 104.09, 101.50, 56.20. Elemental analysis: calculated for $C_{33}H_{25}N_5O_4$, %: C, 71.34; H, 4.54; N, 12.61; O, 11.52. Found, %: C, 72.42; H, 4.37; N, 12.13; O, 11.08. ESI-MS *(m/z)*: calculated for $C_{33}H_{25}N_5O_4$, 555.58 $[M]^+$; found 555.50 $[M + H]^+$.

Additional information on methods can be found in the supplementary information.

Results and discussion

Synthesis

4,6-Di(9*H*-carbazol-9-yl)pyrimidine-5-carbonitrile (**CzPCN**), 4,6-bis(3,6-di-*tert*-butyl-9*H*-carbazol-9-yl)pyrimidine-5-carbonitrile (***t*CzPCN**) and 4,6-bis(3,6-dimethoxy-9*H*-carbazol-9-yl)pyrimidine-5-carbonitrile (**MeOCzPCN**) were obtained by simple and inexpensive synthesis in one step *via* nucleophilic substitution reactions between 4,6-dichloropyrimidine-5-carbonitrile and carbazole derivatives. The synthetic route for the target compounds is outlined in Scheme 1. The chemical structures of the compounds were confirmed by ^{1}H and ^{13}C NMR spectroscopies, mass spectrometry and elemental analysis (SI).

Thermal, electrochemical, photoelectrical and charge-transporting properties

Thermal transitions of the synthesized compounds were investigated by thermogravimetric analysis (TGA) and differential scanning calorimetry (DSC). The results of measurements are collected in Table 1 and showed in Fig. 1*a,b*, S1. All the compounds demonstrated high thermal stability. Their values of 5% weight loss temperatures (T_d) significantly exceeded 300 °C (Fig. 1*a*). In comparison to compound **CzPCN** with T_d of 338 °C, compounds ***t*CzPCN** and **MeOCzPCN** exhibited higher T_d values of 396 °C and of 383 °C respectively. Apparently, the presence of heavy *tert*-butyl and methoxy groups in molecular structures of compounds ***t*CzPCN** and **MeOCzPCN** lead to enhancement of intermolecular interaction in the solid state. Complete weigh loss of **CzPCN** in TGA shows that the compound experienced sublimation.

All the compounds were obtained as crystalline substances after synthesis and showed two melting points in the first DSC scans (Fig. 1*b*, S1, Table 1). It can be assumed that two crystal forms of the synthesized compounds were obtained [37,38]. In the second heating scan of compound **CzPCN** (Fig. 1b) glass transition was observed at 112 °C. The further heating revealed crystallization (the temperature of crystallization (T_{cr}) was of 163 °C) and melting of only one type of polymorph at 273 °C. T_g of 177 °C was observed for compound ***t*CzPCN** in the repeated heating scan (Fig. S1b) while compound **MeOCzPCN** (Fig. S1c) did not show any capability of glass formation.

Cyclic voltammetry measurements (CV) were performed for dichloromethane (DCM) solutions of **CzPCN**, ***t*CzPCN** and **MeOCzPCN** with tetra-*n*-butylammonium hexafluorophosphate ($TBAPF_6$) as supporting electrolyte (Fig. 1*c*). Potentials of oxidation (E_{ox}^{onset}) and reduction (E_{red}^{onset}) half-waves and with respect to ferrocene are collected in Table 1. Using E_{ox}^{onset} and E_{red}^{onset}, the values of ionization potential (IP_{CV}) and electron affinity (EA_{CV}) were determined for the solutions of **CzPCN**, ***t*CzPCN** and **MeOCzPCN** (Table 1). The close values of IP_{CV} and EA_{CV} were observed for **CzPCN** and ***t*CzPCN** (5.82, 5.87/2.9, 2.8 eV respectively) for **CzPCN** and ***t*CzPCN** due to the similar electron-donating/electron-accept ing abilities of the building moieties. Lower IP_{CV} value of **MeOCzPN** is attributed to the stronger electron-donating ability of methoxy-substituted carbazole.

Since IP_{CV} and EA_{CV} energies can not be referred to HOMO and LUMO of the studied materials [39], UV photoelectron spectrometry was further used for getting ionization potential (IP_{UPS}) and electron affinity (EA_{UPS}) for their solid-state samples (Fig. 1*d*). The values of EA_{UPS} were calculated by formula $EA_{UPS} = IP_{UPS}$-$E_{transport} = IP_{UPS}$-E_{opt} assuming that the optical gaps (E_{opt}) of solid layers is approximately equal to their transport gaps ($E_{transport}$). The E_{opt} values were taken from low-energy set-on of absorption spectra of the films of **CzPCN**, ***t*CzPCN** and **MeOCzPCN** (Fig. S2). Thus, IP_{UPS} and EA_{UPS} values can be referred to the HOMO and LUMO energies of compounds **CzPCN**, ***t*CzPCN** and **MeOCzPCN** which are required for the design of appropriate structures of optoelectronic devices, OLEDs in particularly (Table 1). Higher IP_{UPS} values of **CzPCN**, ***t*CzPCN** and **MeOCzPCN** were realtive to the corresponding IP_{CV} values were observed. However, the trends of IP_{UPS} and IP_{CV} were practically the same mainly referring to the different donor substitutions. The extension on the donating carbazoles resulted in raising HOMO/LUMO energy levels.

Two representative compounds **CzPCN** and **MeOCzPCN** were selected for investigation of charge-transporting properties at room temperature. Photocurrent transients for their vacuum deposited films were recorded under positive (for holes) and negative (for electrons) polarities in time of flight (TOF) regime (Fig. 2*a*, S3). Despite of strong dispersity observed for the film of **CzPCN**, clear transit times (t_{tr}) under different electric fields could

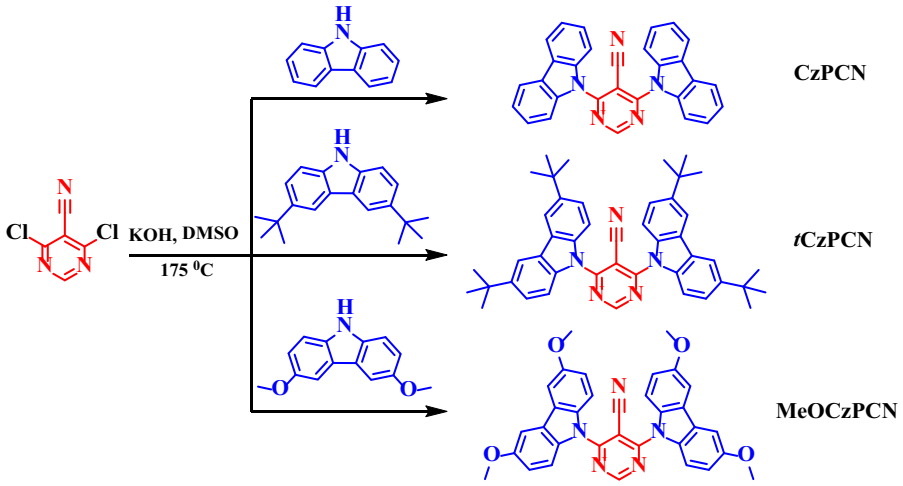

Scheme 1. Synthetic pathway to compounds **CzPCN**, ***t*CzPCN** and **MeOCzPCN**.

Table 1
Thermal, electrochemical and photoelectrical characteristics of **CzPCN**, ***t*CzPCN** and **MeOCzPCN**.

Compounds	T_d,[a] °C	T_g, °C	T_m, °C	T_{cr}, °C	E_{ox}^{onset}, V	E_{red}^{onset}, V	IP_{CV}, eV	EA_{CV}, eV	IP_{UPS}, eV	E_{opt}, eV	EA_{UPS}, eV
CzPCN	338	112[d]	273[b,d]/287[b]	277[b]/163[d]	1.02	− 1.90	5.82	2.90	6.30	2.39	3.91
***t*CzPCN**	396	177[d]	297[b]/326[b]	308[b]	1.07	− 2.00	5.87	2.80	6.10	2.47	3.63
MeOCzPN	383	–	281[b,d]/298[b,d]	283[b]/202[c]	0.76	− 1.20	5.56	3.60	5.86	2.43	3.43

[a] estimated from TGA; DSC: [b] first heating scan, [c] first cooling scan, [d] second heating scan; T_d – the temperature of 5% weight loss; T_g is glass transition temperature; T_m – melting point; T_{cr} – the temperature of crystallization; E_{ox}^{onset} and E_{red}^{onset} are onset oxidation and reduction potentials determined from CV scans of dilute DCM solutions of pyrimidine derivatives; IP_{CV}, IP_{UPS} – ionization potential and EA_{CV}, EA_{UPS} – electron affinity determined from CV and UV photoelectron spectroscopy, respectivly; E_{opt} – optical gap

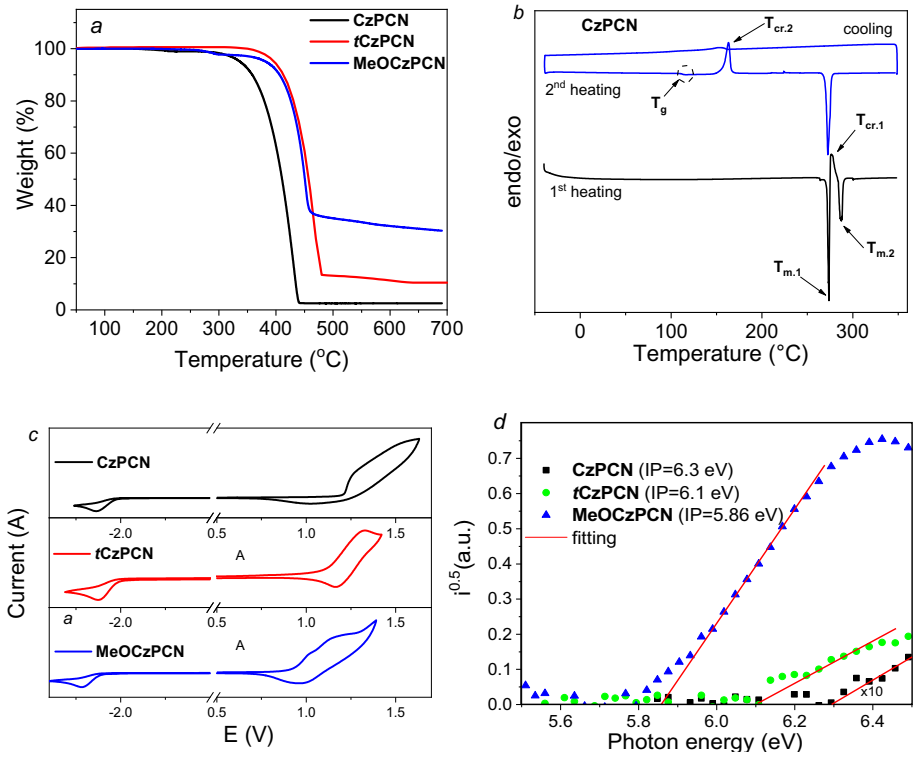

Fig. 1. TGA (*a*) and DSC (*b*) curves, cyclic voltammograms (*c*), and photoelectron emission spectra (*d*) of compounds **CzPCN**, ***t*CzPCN** and **MeOCzPCN**.

be determined for both holes and electrons from the corresponding current transients plotted in log–log scales. Similarly, t_{tr} was detected for electrons for the film of **MeOCzPCN**, while t_{tr} for holes was not detectable. Charge mobilities were calculated for **CzPCN** (for holes and electrons) and for **MeOCzPCN** (for electrons) (Fig. 2*b*). Hole mobility (μ_h) of 1.6 × 10^{-4} $cm^2/V{\cdot}s$ was observed

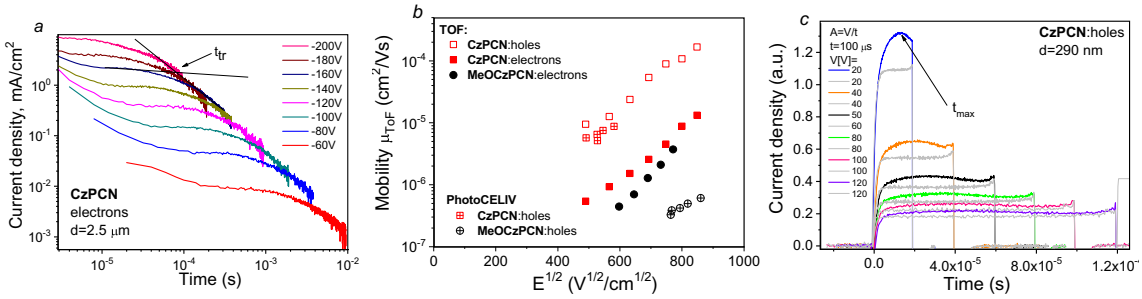

Fig. 2. Photocurrent transients for electrons for the film of compound **CzPCN** (*a*), hole/electron drift mobilities versus electric field (*E*) for the layers of the compounds **CzPCN** and **MeOCzPCN** (*b*), CELIV current transients for holes for the film of **CzPCN** (*c*).

for **CzPCN** at electric field (E) of 7.2 × 10^5 V/cm, which is close to that of many other typical carbazole-containing emitters [33], (Fig. 2*b*). Electron mobility (μ_e) of 1.37 × 10^{-5} cm^2/V·s at the same electric field. It is by ca. one magnitude lower than hole mobility. The relationship $\mu_h > \mu_e$ can be attributed to the donor–acceptor-donor molecular structure of compound **CzPCN** apparently resulting in higher HOMO-HOMO overlapping between neighbouring molecules than LUMO-LUMO overlapping.

Since it was impossible to obtain complete charge-transporting data for the studied compounds by the TOF method, charge extraction by linearly increasing voltage (CELIV) technique was applied using the thinner layers (<300 nm) [40]. The dark-CELIV (grey curves) and photo-CELIV (colour curves) current transients for holes recorded for the film **CzPCN** are plotted in Fig. 2*c*. Taking time t_{max} at the maximum of the photo-CELIV, hole mobilities were obtained for **CzPCN** at different electric fields (Fig. 2*b*). CELIV hole mobility of **CzPCN** was in good agreement with the corresponding TOF hole mobility. CELIV hole mobility was also estimated for the layer of **MeOCzPCN** (Fig. 2*b*).

Photophysical properties

UV absorption and PL spectra of the dilute solutions and of solid films of the **CzPCN**, ***t*CzPCN** and **MeOCzPCN** are presented in Fig. 3*a*, S2. The major photophysical data are summarized in Table 2. The absorption of neat films and dilute toluene solutions of the compounds in the spectral region below 330 nm corresponds to the great extent to π–π* transition of carbazole [41] (Fig. 3*a*). The positions of the lowest energy bands (LEB, Fig. S2) of the dilute solutions observed at ca. 360 nm do not fully correlate with the polarity of solvents. Nevertheless, the significant blue shifts observed for the PL spectra of the solutions in polar solvents such as acetonitrile (MeCN) and acetone relative to the spectra of the solutions in less polar dichloromethane (DCM) and tetrahydrofuran (THF) are attributed to the state of intramolecular CT from carbazole-based donors to the acceptor. Attachment of *tert*-butyl groups to carbazole units in ***t*CzPCN** resulted in the redshift of LEB compared to that of **CzPCN**. Even bigger bathochromic shift was caused by the presence methoxy groups in **MeOCzPCN**. These observations can be explained by prolonged π-conjugation of *tert*-butyl or methoxy substituted carbazole moieties [36]. Intermolecular interactions enhanced in the solid state caused redshifted and broadened LEB of neat films relative to those of the solutions. The E_g values were estimated from the plot presented in Fig. 3*b*. They were found to be of 3.09, 3.08 and 2.9 eV for **CzPCN, *t*CzPCN** and **MeOCzPCN**, respectively. The Kubelka-Munk plot is used for organic semiconductors in solid amorphous layers of OLEDs as they are commonly characterized by a near flat energy bands and direct allowed transitions [42]. The $F(R)\cdot E_{ph}$ plot is based on equation $F(R) = \frac{(1-0.1^A)^2}{2A\cdot 0.1^A}$ F(R) = $\frac{(1-0.1^A)^2}{2A\cdot 0.1^A}$. *A* and E_{ph} stand for absorbance of neat films in our case and photon energy, respectively. *F(R)* is the so-called remission, Kubelka-Munk function.

In order to examine the benefits of tuning emissive properties by electronic excitation energy transfer from host to guest, solid mixtures of the compounds and 1,3-bis(N-carbazolyl)benzene (mCP) with a doping concentration of 10% were investigated. The results are presented in Fig. S2. PL spectra of solutions, doped and non-doped films of the studied compounds contain a single narrow peak in sky-blue/green region with no signs of subvibronic distribution (Fig. 3*a*, S2). Due to guest:host interactions with the weakly polar mCP [43], the difference in energy levels of ground and first excited states of compounds is changed [44] leading to the pronounced blue shifts by 15–40 nm of PL spectra of the films of 10 wt% solid solutions of the compounds in mCP films in comparison with those neat films.

Photoluminescence quantum yields *(Φ)* of toluene solution of **CzPCN** is lower that of THF solution highlighting the intrinsic polarity of the compound and the consequent apparent hypsochromic shift of PL spectrum of the film of the molecular mixture **CzPCN**:mCP compared to that of the film of **CzPCN**. The *Φ* values of the films are higher than those of the solutions which is a mastifestation of AIEE effect. The only exclusion is the *Φ* values observed **MeOCzPCN** which were found to be similar (of ca. 2%) for the solid samples and dilute solutions. The bathochromic shift of PL spectral peak with the increase of polarity of solvents (Fig. S2) is a clear evidence of intramolecular CT state of emission. The solvatochromic effect of absorption and emission of solutions was studied in more in detail for examination of polarity of the compounds. Based on the Onsager interpretation of non-specific interactions between particles and solvent [45], the Lippert-Mataga correlation [46,47] of a Stokes shift $\Delta\nu$ and an orientation polarizability Δf $\Delta\nu = \frac{2\Delta f}{4\pi\varepsilon_0 hca^3}(\mu_e - \mu_g)^2 + \Delta\nu^0$is plotted in Fig. S5 (adjusted R^2 of 0.92–0.97): $\Delta\nu = \frac{2\Delta f}{4\pi\varepsilon_0 hca^3}(\mu_e - \mu_g)^2 + \Delta\nu^0$. The Stokes shift in the condition of absence of solvent is denoted as $\Delta\nu^0$. *a* is an Onsager cavity radius. The obtained slopes are related to the change of dipole moment of compounds in ground μ_g and excited μ_e state revealing a significant intrinsic polarity of the compounds owing to the donor–acceptor-donor structure. The slopes of ca. 9.4·10^3 cm^{-1} observed for **CzPCN** and ***t*CzPCN** are larger than that recorded for **MeOCzPCN** (7.5·10^3 cm^{-1}). Based on these data, **CzPCN** and ***t*CzPCN** can be characterized by stronger intramolecular CT than **MeOCzPCN** showing that for the designed donor–acceptor-donor structures based on the pyrimidine-5-carbonitrile accepting unit attachment of the methoxy groups to carbazoles resulted in suppressing of intramolecular CT and quantum yields.

Thermally activated delayed fluorescence

The intensity of PL of toluene solutions and neat films of the compounds was found to be considerably higher in the absence

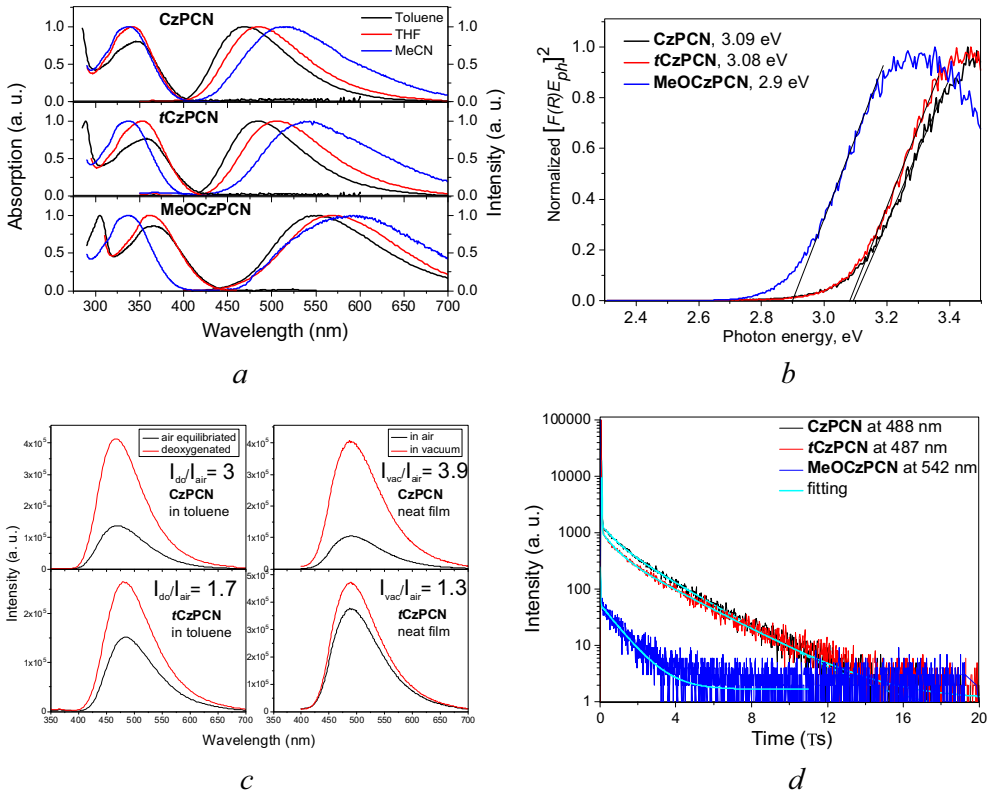

Fig. 3. *a*) Absorption spectra and normalized PL spectra of dilute 10^{-5} M toluene, THF and MeCN solutions of **CzPCN, *t*CzPCN** and **MeOCzPCN**; *b*) Kubelka-Munk plot for neat films; *c*) PL spectra of air equilibrated and deoxygenated dilute 10^{-5} M toluene solutions and of neat films recorded in air and in vacuum; *d*) PL decay curves of neat films.

Table 2
Photophysical characteristics of **CzPCN, *t*CzPCN, MeOCzPCN**.

Compounds/ Parameters	CzPCN	*t*CzPCN	MeOCzPCN
Φ^{touene} (%)	2 (6[¶])	12 (21[¶])	3
Φ^{THF} (%)	15	12	1
$\Phi^{\#}$ (%)	33 (53[¶])	20 (25[¶])	2
$\Phi^{\#}_{PF}$ (%)	14	7	~0.2
$\Phi^{\#}_{DF}$ (%)	39	19[¶]	~1.8
$\tau_{PF}{}^{\#}$ (ns)	12.9	12.2	11.4
$\tau_{DF}{}^{\#}$ (μs)	2.1	2.3	1
$\chi^{2\ \#}$	1.111	1.109	1.016
k_{RISC} (10^6 s^{-1}) [#]	1.56	1.32	–
k_{ISC} (10^7 s^{-1}) [#]	5.73	6.06	–
$E_{S1,\ THF}$ (eV)	3.17	3.02	2.89
$E_{T1,\ THF}$ (eV)	3.03	2.93	2.88
$\Delta E_{ST,\ THF}$ (eV)	0.14	0.09	0.01
$E_{S1,\ mCP}$ (eV)	2.99	2.93	2.74
$E_{T1,\ mCP}$ (eV)	2.91	2.86	2.71
$\Delta E_{ST,\ mCP}$ (eV)	0.08	0.07	0.03

Estimated by the measurements: [#]of neat films; [¶]upon removing oxygen; χ^2 is a weighted sum of squares of deviations of calculated points of multiexponential fitting of a PL decay curve. The empirical formula E_{ph} [eV] = 1239.84/ λ [nm] was used to estimate energy levels of E_{S1} and E_{T1}, where λ is a wavelengths of onset of fluorescence and phosphorescence spectral bands.

of oxygen compared to that of air equilibrated samples (Fig. 3*c*). For **CzPCN** the increase was substantially higher reaching the factor of 3–3.85. The increase of emission intensity after deoxygenation is ascribed to delayed fluorescence (DF) [10]. After removal of oxygen, the spectral shape remained the same. This observation shows, that the excitons utilized in DF are recombined radiatively from the same energy levels as for prompt fluorescence (PF) pointing to the triplet up-conversion via RISC. Supressing interactions between molecules of the studied compounds and oxygen quenches non-radiative pathes of deactivation of excitation via energy thus stimulating RISC.

Multiexponential fitting of PL decay curves (Fig. 3*d*) of neat films of the compounds revealed PF with the lifetime (τ_{PF}) of ca12 ns and DF with the lifetime (τ_{DF}) in a μs range (Table 2). Rate constants of RISC and intersystem crossing (ISC), k_{RISC} and k_{ISC} respectively, can be estimated using formulas $k_{RISC} = \frac{(\Phi_{PF}+\Phi_{DF})\Phi_{RISC}}{\tau_{DF}\Phi_{PF}}$, $k_{ISC} = \frac{\Phi_{DF}}{\tau_{PF}(\Phi_{PF}+\Phi_{DF})}$, where Φ_{PF}, Φ_{DF} and Φ_{RISC} stand for yields of PF, DF and RISC respectively [23]. Knowing $\Phi = \Phi_{PF} + \Phi_{DF} = \frac{\Phi_{PF}}{1-\Phi_{ISC}\Phi_{RISC}}$ and that the maximum value of ISC yield Φ_{ISC} is limited by a quantity of electronic excitation energy not utilized in PF, the equation for estimation of k_{RISC} is simplified to $k_{RISC} = \frac{\Phi_{DF}}{\tau_{DF}\Phi_{PF}(1-\Phi_{PF})}$. Φ_{DF} values are recalculated according to the increase of PL intensity of neat films after degazation (Fig. 3*c*) [48]. The obtained values of k_{RISC} of 1.3–1.6·10^6 s^{-1} and k_{ISC} of ~ 0.6·10^8 s^{-1} for **CzPCN** and ***t*CzPCN** were found to be competitive with the characteristics of TADF emitters such as 1,2,3,5-tetrakis(carbazol-9-yl)-4,6-dicyanobenzene (4CzIPN) [25] or derivatives of pyrimidine-5-carbonitrile and carbazole [36] (Table 2, S1). The fast RISC and ISC are due to satisfactory values of ΔE_{ST} which did not exceed 140 meV. The values of ΔE_{ST} were obtained from the fluorescence and phosphorescence spectra of the solutions of the compounds recorded at liquid nitrogen temperature (Fig. S6, Table 2). The Φ_{DF}/Φ_{PF} of 10.41 was estimated for the film of **MeOCzPCN** in air. This observation explains the failure of the measurement of increase of PL intensity in a vacuum condition, since TADF appeared even in presence of oxygen. Taking into account negative effect of methoxy substitution of carbazoles on overall CT performance and corresponding low Φ values for **MeOCzPCN** it can be presumed, that most of excitons are deactivated through non-radiative ways making the proper estimation of rate constants problematic. The obtained value of k_{RISC} of ~ 10^7 s^{-1}

is an approximated exaggerated to a great extent value. The lowest ΔE_{ST} of 10 meV observed in the series of investigated emitters is suitable for efficient triplet up-conversion partially explaining the obtained high value of k_{RISC} [23].

The solid molecular mixtures of the studied compounds and mCP were studied. Phosphorescence and PL spectra of the doped films correspond to the respective spectra of neat films with the slight redshifts (Fig. S2) caused by dipolar interactions of guest and host. Doping of **CzPCN** and ***t*CzPCN** into mCP matrix resulted in the reduction of ΔE_{ST} as it is linked to the spin-vibronic coupling of local excited and CT states which are strongly affected to the polarity and rigidity of the host [23,49]. Experimental results of the measurements at 77 K are collected in (Table 2).

PL spectra and decay curves of the films of the molecular mixtures were recorded at different temperatures. They are presented in Fig. 4, S7-9. PL spectra the films remained steady over heating when the samples were degassed (Fig. 3*c*). Due to low ΔE_{ST} (up to 80 meV, Table 2), deactivation of excitons occurred via phosphorescence, PF and DF at different temperatures from excited states having similar energy levels, which is typical for compounds exhibiting TADF. As it is evident from PL decay curves, the intensity of phosphorescent component was quenched over heating due to rapidly enhanced interactions with oxygen. Simultaneously, thermal activation of DF resulted in the essential increase of TADF intensity at the temperatures exceeding 180 K.

To exclude triplet–triplet annihilation utilizing higher triplet excited states T_2, T_3 etc., investigation of power dependence of DF was performed (Fig. S10). The linear plot (fitting slope of 0.98–1.04) of the DF integrated intensity versus excitation dose of laser beam in the logarithmic scale in the whole range of intensity of excitation points to TADF.

Aggregation induced emission enhancement

The dispersions of **CzPCN** and ***t*CzPCN** in THF/water mixtures were prepared for investigation of AIEE characteristics of the compounds. The dependencies of PL intensities on water fraction are shown in Fig. 4*c*,*d*. The PL spectra and the relative correlation of the peak wavelengths and emission intensities are presented in Fig. S11. As it may be seen from the graphs and photos (Fig. 4*c*, *d*), at low water fractions (f_w) the dispersions of both the compounds are poorly emissive. Decrease of PL intensity in the range f_w below 40% is ascribed to the emission quenching due to an exhaustion of electronic excitation energy by intramolecular rotations. The bathochromic shift by nearly 50 nm with the increase of water fraction from 0 to 40% is caused by the increase of concentration of highly polar water influencing strong intramolecular CT processes in the emitters which is an additional reason of PL quenching. At high f_w both compounds emit blue light with the intensity maxima at ca.480 nm as the molecules being insoluble in water form aggregates. Consequently, there is a rapid increase of intensity at f_w > 70% for the dispersions of **CzPCN** and for ***t*CzPCN** in the range of f_w from 40 to 60% due to AIEE since the rotation motions of moieties of the compounds are restricted in solid state. The following decrease of PL intensity at f_w exceeding 70% observed for the dispersion of ***t*CzPCN** is explained by the formation of precipitates of a significant size. It is important to note that obtained results do not necessarily mean the decrease of Φ upon aggregation for the dispersions of ***t*CzPCN** in THF/water mixtures at high f_w.

Performance in OLEDs

Taking into account TADF and AIEE capabilities as well as bipolar charge transport and appropriate HOMO/LUMO levels for charge injections from electrodes, the synthesized compounds can be regarded as promising for doping free devices. The series of OLEDs N1-N3 with the structure of ITO / HAT-CN (10 nm) / TCTA (30 nm) / mCP (7 nm) / EML (25 nm) / TSPO1 (3 nm) / TPBi (30 nm) / LiF (0.4 nm) / Al were fabricated in order to test the layers of **CzPCN**, ***t*CzPCN** and **MeOCzPCN** as non-doped light-emitting layers, respectively. Major electroluminescent data are collected in

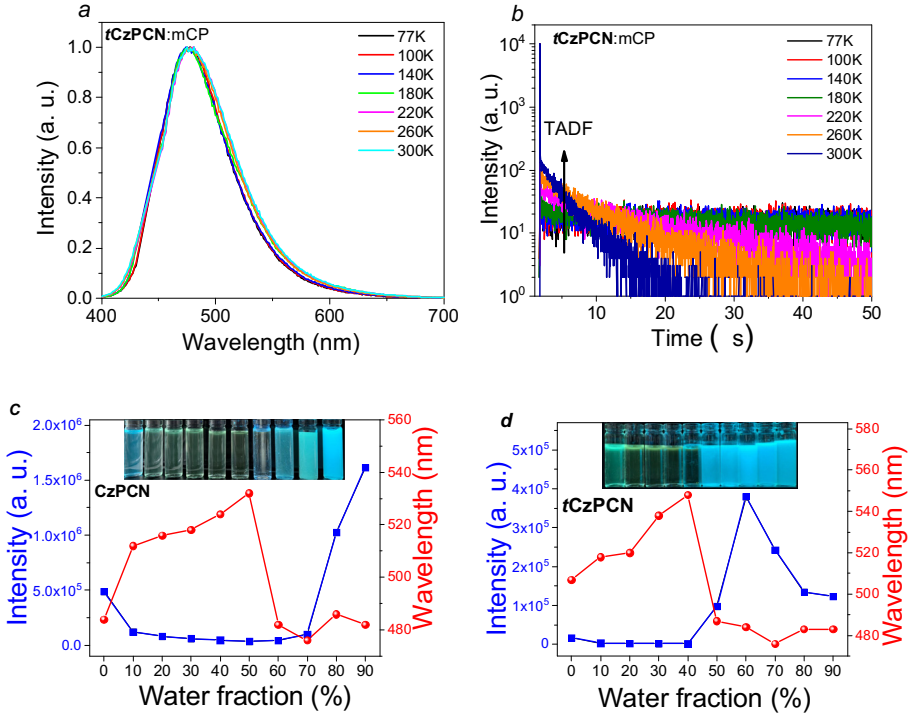

Fig. 4. Normalized PL spectra (*a*) and PL decay curves (*b*) recorded at the different temperatures under N_2 atmosphere for 10 wt% solid solution of ***t*CzPCN** in mCP. Plots of PL intensities and peak wavelengths versus f_w of the dispersions of **CzPCN** (*c*) and ***t*CzPCN** (*d*) in THF/water mixtures.

Table 3, Fig. 5, S12. Dipyrazino[2,3-f:2′,3′-h]quinoxaline-2,3,6,7,10,11-hexacarbonitrile (HAT-CN) and LiF were employed for the injection of charge carriers. The layers of tris(4-carbazoyl-9-ylphenyl)amine (TCTA) and 2,2′,2″-(1,3,5-benzinetriyl)-tris(1-phenyl-1-H-benzimidazole) (TPBi) were utilized as the hole and electron transporting layers, respectively. 1,3-bis(N-carbazolyl)benzene (mCP) and diphenyl[4-(triphenylsilyl)phenyl]phosphine oxide (TSPO1) were employed for the blocking electrons and holes, respectively. The electrodes were indium-tin oxide (ITO) and aluminium. For the studied derivatives negative values of IP_{UPS} were taken as a HOMO value and LUMO energy levels were estimated by an addition of E_g calculated from Kubelka-Munk plot to HOMO values (Fig. 5*a*).

The EL spectral characteristics of the compounds are in an accordance with the PL properties (Fig. 3*a*, 5*b*). As it can be seen from EL spectra and corresponding CIE coordinates (Fig. 5*b*, S12), OLEDs containing emitting layers of **CzPCN**, ***t*CzPCN** emit near sky-blue range while **MeOCzPCN** is a totally green emitter.

Taking into account the out-coupling factor, it is evident that the obtained maximum values of EQE of the devices (Table 3) correlate with the values of Φ of the neat films of the compounds (Table 2). This observation is an indication of the excellent charge balance in EML. Device N1 exhibited maximum EQE of 12.8% of which is practically the same as for the corresponding doped device D1 which will be discussed below. Much lower maximum EQE of 5.1% was obtained for the non-doped ***t*CzPCN-**based device **N2** (Table 3).

Aiming to obtain better hole-electron balance within the light-emitting layers, the structure of OLEDs was additionally modified by insertion of guest:host system instead of neat EML. The characteristics of OLEDs based on **CzPCN**, ***t*CzPCN** and **MeOCzPCN** 10 wt% doped into mCP were investigated in detail. The series of devices D1-D3 respectively were fabricated. As it was mentioned above, device D1 showed a slight improvement of efficiency compared device N1. Meanwhile, efficiency of OLED D2 was significantly higher than that of N2 (EQE of 5.1 and 13.7%). This observation can apparently be attributed to better hole-electron balance in doped light-emitting layer of device D2 compared to that of non-doped device N2.

Unlike OLEDs with neat films of **CzPCN** and ***t*CzPCN**, devices with doped EML of these emitters exhibited practically close to identical efficiencies and EL spectra. High efficiency OLED based on EML of ***t*CzPCN** doped in mCP can be additionally explained by suppression of non-radiative ways of relaxation of excited states. Analogous improvement was not achieved for device based on the emitter with methoxy groups since this derivative exhibited low photoluminescence quantum yield (Table 2). Efficiency roll-off evident form the rapid decline of efficiency at 100 cd/m^2 of L is bigger for device D3 than for N3 despite the exhibition of the same maximum EQE of 1.4%. This observation can apparently be explained by the non-ideal host–guest interaction. The incomplete energy transfer from host to **MeOCzPCN** is manifested by the presence of EL spectral band of D3 at ca.380 nm, typical for mCP [50]. It also caused a substantial shift of CIE coordinates to those of blue color.

Oxygen sensitivity

Interactions with oxygen are mostly responsible for the non-radiative deactivation of excitations through the energy losses. Taking pronounced AIEE properties into account, and high values of photoluminescence quantum yield in solid-state, **CzPCN** and ***t*CzPCN** were selected for the investigation of the optical oxygen sensitivity. The 10 wt% solid solutions of the compounds in rigid matrix were prepared to detect collisional quenching of a luminophore. Zeonex® was selected as a matrix because of its well-studied ability of supressing intermolecular interactions [51–53]. The samples were put into an inert atmosphere of nitrogen. Upon increasing of oxygen concentration the PL intensity continuously dropped (Fig. 6*a*,*b*, S14). No any significant difference in intensity in the same conditions over time was detected showing a great immediate response to the molecules of oxygen and a great stability of the emission.

PL decay curves of the solid solutions of **CzPCN** and ***t*CzPCN** in Zeonex® were recorded under nitrogen and oxygen conditions to study the impact of collisional quenching on emissive characteristics of the systems (Fig. 6*c*, S13). The long-lived component of the emission was drastically reduced in the presence of oxygen, espe-

Table 3
Summary of OLED parameters.

OLED	EML	L_{max}, 10^{3}cd/m^2	η_c, cd/A	η_p, lm/W	λ_{EL}, nm	EQE, %	CIE 1931
N1	**CzPCN**	13.1	32.4 (17.5)	18.8 (9.2)	494	12.8 (6.9)	(0.20, 0.36)
D1	**CzPCN**:mCP	23.1	33.3 (17.6)	20.2 (9.1)	489	14 (7.4)	(0.18, 0.33)
N2	***t*CzPCN**	13.2	12.3 (9.9)	4.6 (3.6)	490	5.1 (4.1)	(0.19, 0.35)
D2	***t*CzPCN**:mCP	14.8	33.7 (19.4)	18 (8.7)	490	13.7 (7.9)	(0.18, 0.35)
N3	**MeOCzPCN**	9.3	4.0 (3.4)	2.1 (1.6)	524	1.4 (1.2)	(0.30, 0.49)
D3	**MeOCzPCN**:mCP	13.7	3.8 (0.6)	1.2 (0.3)	500	1.4 (0.2)	(0.21, 0.43)

L_{max} – maximum brightness. η_c and η_p – maximum current and power efficiency, respectively. λ_{EL} – wavelength of EL spectral peak at 8 V. Efficiency values at L of 100 cd/m^2 are showed in parentheses.

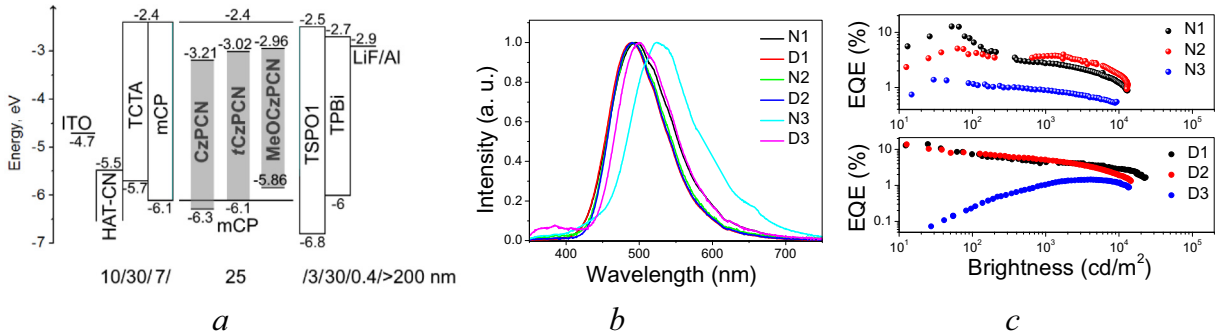

Fig. 5. OLEDs N1-N3 and D1-D3: *a*) Equilibrium energy diagram and structure; *b*) normalized EL spectra recorded at 8 V; *c*) EQE.

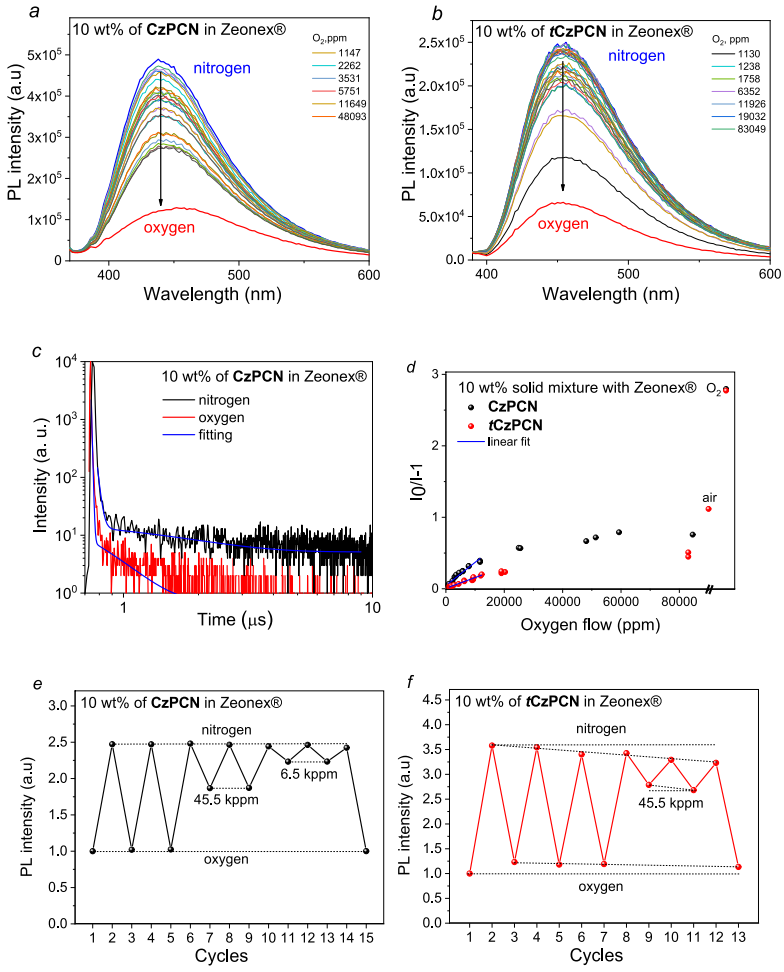

Fig. 6. PL spectra (*a, b*) and PL decays (*c*) of 10 wt% solid solutions of **CzPCN** (*a, c*) or ***t*CzPCN** (*b*) in Zeonex® recorded in different atmosphere at room temperature; *d*) Stern-Volmer plots and oxygen response (*e, f*) of the films of 10 wt% solid solutions of **CzPCN** (*e*) and ***t*CzPCN** (*f*) in Zeonex®.

cially for the solid solutions of **CzPCN**. In PL decay curve of the solid solution of this compound DF is almost absent. Stern-Volmer relation of $\frac{I_0}{I} - 1$ and oxygen flow (Fig. 6*d*) demonstrated the oxygen sensitivity in the wide range of the oxygen flow corresponding to the oxygen partial pressure [54]. Since the fluorophore quenching by oxygen is a dynamic process, the correlation is linear. However, as expected for dye:matrix systems, downward curvature [48] takes place at the oxygen flow exceeding 20000 ppm. According to the Stern-Volmer equation, the well-known characteristic of optical sensors Stern-Volmer constant $K_{SV} = \frac{I_0}{I} - 1$ was estimated from the slope of the linear fit as it is shown in Fig. 6*d* (adjusted R^2 are 0.94 and 0.97 for the samples containing **CzPCN** and ***t*CzPCN**, respectively) [48]. K_{SV} was calculated to be $3.24 \cdot 10^{-5}$ and $1.49 \cdot 10^{-5}$ ppm^{-1} for the solid dispersions of **CzPCN** and ***t*CzPCN** in Zeonex®, respectively. These values are comparable with that of TADF oxygen probes [55]. They are slightly lower than K_{SV} values earlier observed for phosphorescent oxygen probes with long-lived emission (>1 ms) [56,57]. Taking into account that the oxygen sensing properties correlate with TADF, thermal motions of molecules activate RISC at elevated temperatures and consequently the oxygen sensitivity is expected to be enhanced [19]. The synthesized compounds have a great potential for the application as optical oxygen sensors reaching necessary requirements: a) fast response to the oxygen postulated from the stability of PL quenching over time; b) sustainable oxygen sensitivity; c) good quality of the films of solid dispersions in Zeonex®; d) appropriate thermal stability and photophysical properties described above [48].

Conclusions

Exploiting donor–acceptor-donor molecular structure, simple cost-effective synthesis of new sky-blue luminophores containing pyrimidine-5-carbonitrile electron-withdrawing scaffold and electron-donating carbazole, *tert*-butylcarbazole or methoxy carbazole moieties were developed. Using the synthesized compounds as blue emitters, maximum external quantum efficiencies of 12.8 and 14% of were achieved for non-doped and doped electroluminescent devices respectively. Such performances were observed due to bipolar charge transport, thermal stability, and high photoluminescent quantum efficiency in solid state of the newly developed emitters. The different donor substitution of pyrimidine-5-carbonitrile unit affects the thermally activated delayed fluorescence and aggregation-induced emission enhancement properties of the compounds giving a path for oxygen sensor application. The developed oxygen sensor showed good sensitivity characterized by Stern-Volmer constant of $3.24 \cdot 10^{-5}$ ppm^{-1}. They were characterized by high stability and repeatability of the sensitivity.

Declaration of Competing Interest

The authors declare that they have no known competing financial interests or personal relationships that could have appeared to influence the work reported in this paper.

Acknowledgements

This project has received funding from European Regional Development Fund (project No 01.2.2-LMT-K-718-01-0015) under grant agreement with the Research Council of Lithuania (LMTLT).

Appendix A. Supplementary data

Supplementary data to this article can be found online at https://doi.org/10.1016/j.jare.2021.01.014.

References

[1] Savage N. Tomorrow's industries: from OLEDs to nanomaterials. Nature 2019;576:S20–2. doi: https://doi.org/10.1038/d41586-019-03764-1.
[2] Leo K. Organic light-emitting diodes: Efficient and flexible solution. Nat Photonics 2011;5:716–8. doi: https://doi.org/10.1038/nphoton.2011.288.
[3] Gregory JW, Asai K, Kameda M, Liu T, Sullivan JP. A review of pressure-sensitive paint for high-speed and unsteady aerodynamics. Proc Inst Mech Eng Part G J Aerosp Eng 2008;222:249–90. doi: https://doi.org/10.1243/09544100JAERO243.
[4] Gregory JW, Sakaue H, Liu T, Sullivan JP. Fast pressure-sensitive paint for flow and acoustic diagnostics. Annu Rev Fluid Mech 2014;46:303–30. doi: https://doi.org/10.1146/annurev-fluid-010313-141304.
[5] Huang CY, Matsuda Y, Gregory JW, Nagai H, Asai K. The applications of pressure-sensitive paint in microfluidic systems. Microfluid Nanofluidics 2015;18:739–53. doi: https://doi.org/10.1007/s10404-014-1510-z.
[6] Matsuda Y, Uchida T, Suzuki S, Misaki R, Yamaguchi H, Niimi T. Pressure-sensitive molecular film for investigation of micro gas flows. Microfluid Nanofluidics 2011;10:165–71. doi: https://doi.org/10.1007/s10404-010-0664-6.
[7] Yersin H. Highly Efficient OLEDs with Phosphorescent Materials 2008. doi: https://doi.org/10.1002/9783527621309.
[8] Minaev B, Baryshnikov G, Agren H. Principles of phosphorescent organic light emitting devices. PCCP 2014;16:1719–58. doi: https://doi.org/10.1039/c3cp53806k.
[9] Tao Y, Yuan K, Chen T, Xu P, Li H, Chen R, et al. Thermally activated delayed fluorescence materials towards the breakthrough of organoelectronics. Adv Mater 2014;26:7931–58. doi: https://doi.org/10.1002/adma.201402532.
[10] Adachi C. Third-generation organic electroluminescence materials. Jpn J Appl Phys 2014;53. doi: https://doi.org/10.7567/JJAP.53.060101.
[11] Uoyama H, Goushi K, Shizu K, Nomura H, Adachi C. Highly efficient organic light-emitting diodes from delayed fluorescence. Nature 2012;492:234–8. doi: https://doi.org/10.1038/nature11687.
[12] Minaev B. Photochemistry and spectroscopy of singlet oxygen in solvents. Recent advances which support the old theory. Chem Chem Technol 2016;10:519–30.
[13] Paisley NR, Tonge CM, Hudson ZM. Stimuli-Responsive Thermally Activated Delayed Fluorescence in Polymer Nanoparticles and Thin Films: Applications in Chemical Sensing and Imaging. Front Chem 2020;8. doi: https://doi.org/10.3389/fchem.2020.00229.
[14] Méhes G, Nomura H, Zhang Q, Nakagawa T, Adachi C. Enhanced electroluminescence efficiency in a spiro-acridine derivative through thermally activated delayed fluorescence. Angew Chemie - Int Ed 2012;51:11311–5. doi: https://doi.org/10.1002/anie.201206289.
[15] Kochmann S, Baleizão C, Berberan-Santos MN, Wolfbeis OS. Sensing and imaging of oxygen with parts per Billion limits of detection and based on the quenching of the delayed fluorescence of 13C 70 fullerene in polymer hosts. Anal Chem 2013;85:1300–4. doi: https://doi.org/10.1021/ac303486f.
[16] Berberan-Santos MN, Garcia JMM. Unusually strong delayed fluorescence of C70. J Am Chem Soc 1996;118:9391–4. doi: https://doi.org/10.1021/ja961782s.
[17] Matsuda Y, Ueno K, Yamaguchi H, Egami Y, Niimi T. Organic electroluminescent sensor for pressure measurement. Sensors (Switzerland) 2012;12:13899–906. doi: https://doi.org/10.3390/s121013899.
[18] Giebink NC, D'Andrade BW, Weaver MS, MacKenzie PB, Brown JJ, Thompson ME, et al. Intrinsic luminance loss in phosphorescent small-molecule organic light emitting devices due to bimolecular annihilation reactions. J Appl Phys 2008;103. doi: https://doi.org/10.1063/1.2884530.
[19] Ogiwara T, Wakikawa Y, Ikoma T. Mechanism of intersystem crossing of thermally activated delayed fluorescence molecules. J Phys Chem A 2015;119:3415–8. doi: https://doi.org/10.1021/acs.jpca.5b02253.
[20] Zhang Q, Li B, Huang S, Nomura H, Tanaka H, Adachi C. Efficient blue organic light-emitting diodes employing thermally activated delayed fluorescence. Nat Photonics 2014;8:326–32. doi: https://doi.org/10.1038/nphoton.2014.12.
[21] Wong MY, Zysman-Colman E. Purely Organic Thermally Activated Delayed Fluorescence Materials for Organic Light-Emitting Diodes. Adv Mater 2017;29. doi: https://doi.org/10.1002/adma.201605444.
[22] Dias FB, Bourdakos KN, Jankus V, Moss KC, Kamtekar KT, Bhalla V, et al. Triplet harvesting with 100% efficiency by way of thermally activated delayed fluorescence in charge transfer OLED emitters. Adv Mater 2013;25:3707–14. doi: https://doi.org/10.1002/adma.201300753.
[23] Dias FB, Penfold TJ, Monkman AP. Photophysics of thermally activated delayed fluorescence molecules. Methods Appl Fluoresc 2017;5. doi: https://doi.org/10.1088/2050-6120/aa537e.
[24] Liu Y, Li C, Ren Z, Yan S, Bryce MR. All-organic thermally activated delayed fluorescence materials for organic light-emitting diodes. Nat Rev Mater 2018;3. doi: https://doi.org/10.1038/natrevmats.2018.20.
[25] Hosokai T, Matsuzaki H, Nakanotani H, Tokumaru K, Tsutsui T, Furube A, et al. Evidence and mechanism of efficient thermally activated delayed fluorescence promoted by delocalized excited states. Sci Adv 2017;3. doi: https://doi.org/10.1126/sciadv.1603282.
[26] Chan CY, Cui LS, Kim JU, Nakanotani H, Adachi C. Rational Molecular Design for Deep-Blue Thermally Activated Delayed Fluorescence Emitters. Adv Funct Mater 2018;28. doi: https://doi.org/10.1002/adfm.201706023.
[27] Stokes GG. LXI. On the metallic reflexion exhibited by certain non-metallic substances . London, Edinburgh, Dublin Philos Mag J Sci 1853;6:393–403. https://doi.org/10.1080/14786445308647395.
[28] Luo J, Xie Z, Xie Z, Lam JWY, Cheng L, Chen H, et al. Aggregation-induced emission of 1-methyl-1,2,3,4,5-pentaphenylsilole. Chem Commun 2001;18:1740–1. doi: https://doi.org/10.1039/b105159h.
[29] Chen Y, Lam JWY, Kwok RTK, Liu B, Tang BZ. Aggregation-induced emission: Fundamental understanding and future developments. Mater Horizons 2019;6:428–33. doi: https://doi.org/10.1039/c8mh01331d.
[30] Guo J, Zhao Z, Tang BZ. Purely Organic Materials with Aggregation-Induced Delayed Fluorescence for Efficient Nondoped OLEDs. Adv Opt Mater 2018;6. doi: https://doi.org/10.1002/adom.201800264.
[31] Danyliv Y, Lytvyn R, Volyniuk D, Bezvikonnyi O, Hladka I, Grazulevicius JV. Derivatives of carbazole and chloropyridine exhibiting aggregation induced emission enhancement and deep-blue delayed fluorescence. Dye Pigment 2018;149:588–96. doi: https://doi.org/10.1016/j.dyepig.2017.11.027.
[32] Rizzo F, Cucinotta F. Recent Developments in AIEgens for Non-doped and TADF OLEDs. Isr J Chem 2018;58:874–88. doi: https://doi.org/10.1002/ijch.201800049.
[33] Wex B, Kaafarani BR. Perspective on carbazole-based organic compounds as emitters and hosts in TADF applications. J Mater Chem C 2017;5:8622–53. doi: https://doi.org/10.1039/c7tc02156a.
[34] Kimoto A, Cho JS, Higuchi M, Yamamoto K. Synthesis of asymmetrically arranged dendrimers with a carbazole dendron and a phenylazomethine dendron. Macromolecules 2004;37:5531–7. doi: https://doi.org/10.1021/ma0499674.
[35] Serevičius T, Skaisgiris R, Fiodorova I, Steckis V, Dodonova J, Banevičius D, et al. Achieving efficient deep-blue TADF in carbazole-pyrimidine compounds. Org Electron 2020;82. doi: https://doi.org/10.1016/j.orgel.2020.105723.
[36] Jang JS, Lee HL, Lee KH, Lee JY. Electrostatic potential dispersing pyrimidine-5-carbonitrile acceptor for high efficiency and long lifetime thermally activated delayed fluorescence organic light-emitting diodes. J Mater Chem C 2019;7:12695–703. doi: https://doi.org/10.1039/c9tc04304g.
[37] Hladka I, Volyniuk D, Bezvikonnyi O, Kinzhybalo V, Bednarchuk TJ, Danyliv Y, et al. Polymorphism of derivatives of tert -butyl substituted acridan and perfluorobiphenyl as sky-blue OLED emitters exhibiting aggregation induced thermally activated delayed fluorescence. J Mater Chem C 2018;6:13179–89. doi: https://doi.org/10.1039/c8tc04867c.
[38] Galer P, Korošec RC, Vidmar M, Šket B. Crystal structures and emission properties of the BF2 complex 1-phenyl-3-(3,5-dimethoxyphenyl)-propane-1,3-dione: Multiple chromisms, aggregation- or crystallization-induced emission, and the self-assembly effect. J Am Chem Soc 2014;136:7383–94. doi: https://doi.org/10.1021/ja501977a.
[39] Bredas JL. Mind the gap!. Mater Horizons 2014;1:17–9. doi: https://doi.org/10.1039/c3mh00098b.
[40] Pivrikas A, Sariciftci NS, Juška G, Österbacka R. A review of charge transport and recombination in polymer/fullerene organic solar cells. Prog Photovoltaics Res Appl 2007;15:677–96. doi: https://doi.org/10.1002/pip.791.
[41] Siraj N, Das S, Hasan F, Lu C, Kiruri LW, Steege Gall KE, et al. Enhanced S2 emission in carbazole-based ionic liquids. RSC Adv 2015;5:9939–45. doi: https://doi.org/10.1039/c4ra12362j.
[42] Liu J. Deep-blue efficient OLED based on NPB with little efficiency roll-off under high current density. Appl Phys A Mater Sci Process 2017;123. doi: https://doi.org/10.1007/s00339-017-0840-6.
[43] Zhang Y, Li Z, Li C, Wang Y. Suppressing efficiency roll-off of TADF based OLEDs by constructing emitting layer with dual delayed fluorescence. Front Chem 2019;7. doi: https://doi.org/10.3389/fchem.2019.00302.
[44] Jeon SK, Park HJ, Lee JY. Blue-shifted emission color and high quantum efficiency in solution-processed blue thermally activated delayed fluorescence organic light-emitting diodes using an intermolecular interaction suppressing host decorated with blocking groups. J Mater Chem C 2018;6:6778–83. doi: https://doi.org/10.1039/c8tc02050g.
[45] Onsagbr L. Electric Moments of Molecules in Liquids. J Am Chem Soc 1936;58:1486–93. doi: https://doi.org/10.1021/ja01299a050.
[46] Mataga N, Kaifu Y, Koizumi M. Solvent Effects upon Fluorescence Spectra and the Dipolemoments of Excited Molecules. Bull Chem Soc Jpn 1956;29:465–70. doi: https://doi.org/10.1246/bcsj.29.465.
[47] Sumalekshmy S, Gopidas KR. Photoinduced Intramolecular Charge Transfer in Donor-Acceptor Substituted Tetrahydropyrenes. J Phys Chem B 2004;108:3705–12. doi: https://doi.org/10.1021/jp022549l.
[48] Santos PL, Ward JS, Data P, Batsanov AS, Bryce MR, Dias FB, et al. Engineering the singlet-triplet energy splitting in a TADF molecule. J Mater Chem C 2016;4:3815–24. doi: https://doi.org/10.1039/c5tc03849a.

[49] Etherington MK, Gibson J, Higginbotham HF, Penfold TJ, Monkman AP. Revealing the spin-vibronic coupling mechanism of thermally activated delayed fluorescence. Nat Commun 2016;7. doi: https://doi.org/10.1038/ncomms13680.

[50] Wu Q, Zhang S, Yue S, Zhang Z, Xie G, Zhao Y, et al. Enhanced efficiency in single-host white organic light-emitting diode by triplet exciton conversion. J Lumin 2013;143:108–12. doi: https://doi.org/10.1016/j.jlumin.2013.04.037.

[51] Hayduk M, Riebe S, Voskuhl J. Phosphorescence Through Hindered Motion of Pure Organic Emitters. Chem - A Eur J 2018;24:12221–30. doi: https://doi.org/10.1002/chem.201800521.

[52] Ward JS, Nobuyasu RS, Batsanov AS, Data P, Monkman AP, Dias FB, et al. The interplay of thermally activated delayed fluorescence (TADF) and room temperature organic phosphorescence in sterically-constrained donor-acceptor charge-transfer molecules. Chem Commun 2016;52:2612–5. doi: https://doi.org/10.1039/c5cc09645f.

[53] Kabe R, Adachi C. Organic long persistent luminescence. Nature 2017;550. doi: https://doi.org/10.1038/nature24010.

[54] Narayanaswamy R, Wolfbeis OS. Optical Sensors: Industrial Environmental and Diagnostic Applications. vol. 1. 2004. https://doi.org/10.1007/978-3-662-09111-1.

[55] Steinegger A, Klimant I, Borisov SM. Purely Organic Dyes with Thermally Activated Delayed Fluorescence—A Versatile Class of Indicators for Optical Temperature Sensing. Adv Opt Mater 2017;5. doi: https://doi.org/10.1002/adom.201700372.

[56] Yoshihara T, Yamaguchi Y, Hosaka M, Takeuchi T, Tobita S. Ratiometric molecular sensor for monitoring oxygen levels in living cells. Angew Chemie - Int Ed 2012;51:4148–51. doi: https://doi.org/10.1002/anie.201107557.

[57] Zach PW, Freunberger SA, Klimant I, Borisov SM. Electron-Deficient Near-Infrared Pt(II) and Pd(II) Benzoporphyrins with Dual Phosphorescence and Unusually Efficient Thermally Activated Delayed Fluorescence: First Demonstration of Simultaneous Oxygen and Temperature Sensing with a Single Emitter. ACS Appl Mater Interfaces 2017;9:38008–23. doi: https://doi.org/10.1021/acsami.7b10669.